OPEN ACCESS

Biomedicine ARTICLE

The Innovation Life

Topology-enabled long-acting interleukin-2 for advanced low-dose interleukin-2 therapy of autoimmune diseases

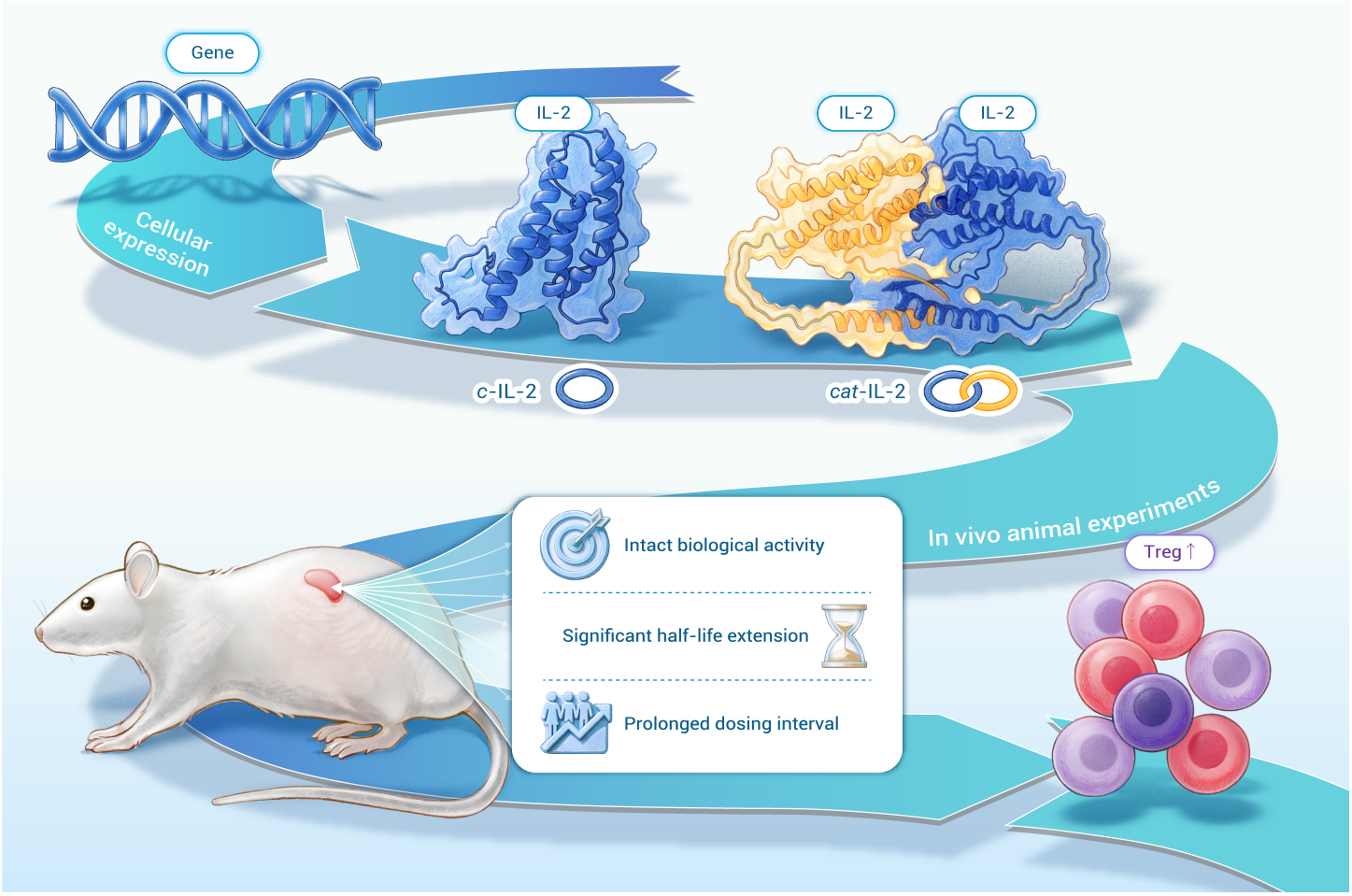
Jing Fang,[1,2,3,4,9] Ruiling Feng,[5,6,9] Xibao Tian,[1,2,3,4,9] Xian Xiao,[5,6,9] Bo Huang,[5,6] Yuange Duan,[7] Jian Lu,[8] Zhanguo Li,[5,6,*] Wen-Bin Zhang,[1,2,3,4,5,*] and Jing He[5,6,*]

*Correspondence: wenbin@pku.edu.cn (W. Z.); hejing1105@126.com (J.H.); li99@bjmu.edu.cn (Z.L.)

Received: February 2, 2026; Accepted: September 21, 2026; Published Online: September 28, 2026; https://doi.org/10.59717/j.xinn-life.2026.100259

© 2026 The Author(s). This is an open access article under the CC BY license (https://creativecommons.org/licenses/by/4.0/).

GRAPHICAL ABSTRACT



PUBLIC SUMMARY

- Cyclic and catenated interleukin-2 (IL-2) with intact bioactivity are directly synthesized in living cells.
- These variants induce preferential Treg expansion to rebalance immunity.
- Extended serum half-life enables weekly low-dose treatment for three autoimmune diseases.
- Topology engineering overcomes protein therapeutic limits, offering a platform for next-generation biologics.

ARTICLE Biomedicine

OPEN ACCESS

www.the-innovation.org/the-innovation-life

Topology-enabled long-acting interleukin-2 for advanced low-dose interleukin-2 therapy of autoimmune diseases

Jing Fang,[1,2,3,4,9] Ruiling Feng,[5,6,9] Xibao Tian,[1,2,3,4,9] Xian Xiao,[5,6,9] Bo Huang,[5,6] Yuange Duan,[7] Jian Lu,[8] Zhanguo Li,[5,6,*] Wen-Bin Zhang,[1,2,3,4,5,*] and Jing He[5,6,*]

[1]Beijing National Laboratory for Molecular Sciences, Peking University, Beijing 100871, China

[2]Key Laboratory of Polymer Chemistry & Physics of Ministry of Education, Peking University, Beijing 100871, China

[3]Center for Soft Matter Science and Engineering, Peking University, Beijing 100871, China

[4]College of Chemistry and Molecular Engineering, Peking University, Beijing 100871, China

[5]Beijing Key Laboratory of Non-invasive Diagnosis and Immunotherapy of Rheumatic Diseases, Peking University People's Hospital, Beijing 100044, China

[6]Department of Rheumatology and Immunology, Peking University People's Hospital, Beijing 100044, China

[7]Key Laboratory of Pest Monitoring and Green Management, Department of Entomology, College of Plant Protection, China Agricultural University, Beijing 100193, China

[8]State Key Laboratory of Protein and Plant Gene Research, Center for Bioinformatics, School of Life Sciences, Peking University, Beijing 100871, China

[9]These authors contributed equally to the work

*Correspondence: wenbin@pku.edu.cn (W. Z.); hejing1105@126.com (J.H.); li99@bjmu.edu.cn (Z.L.)

Received: February 2, 2026; Accepted: September 21, 2026; Published Online: September 28, 2026; https://doi.org/10.59717/j.xinn-life.2026.100259

© 2026 The Author(s). This is an open access article under the CC BY license (https://creativecommons.org/licenses/by/4.0/).

Citation: Fang J., Feng R., Tian X., et al. (2026). Topology-enabled long-acting interleukin-2 for advanced low-dose interleukin-2 therapy of autoimmune diseases. *The Innovation Life* **4**:100259.

The therapeutic efficacy of protein biologics is often hampered by their rapid *in vivo* degradation and off-target effects. Interleukin-2 (IL-2), a cytokine promising for treating autoimmune diseases via regulatory T cell (Treg) expansion, exemplifies this challenge due to its short half-life and pleiotropic activity. Herein, we report a molecular-scale topology engineering strategy to overcome these limitations. By using split intein mediated ligation and genetically encoded entangling motif, p53dim (X), we constructed cyclic (*c*-IL-2) and catenated (*cat*-IL-2) variants of IL-2 via direct expression in *E. coli*. These topological proteins preserve the native conformation and receptor binding capacity of IL-2 with minimal to minor exogenous motifs, while exhibiting superior proteolytic stability and a dramatically extended serum half-life (approximately 4.5–5.0-fold longer than wt-IL-2). In murine models of three distinct autoimmune diseases (lupus, rheumatoid arthritis, and Sjögren's syndrome), weekly administration of these topological IL-2 variants effectively rebalanced immunity, as evidenced by a marked expansion of Tregs and significant amelioration of tissue injury and clinical biomarkers. Transcriptomic profiling confirmed the induction of a tolerogenic program without systemic toxicity. This work establishes protein topology engineering as a minimalist, yet robust and generalizable platform to enhance the pharmacokinetics and functional specificity of therapeutic proteins, offering a powerful new modality for biologic drug development.

INTRODUCTION

Autoimmune diseases (ADs), such as systemic lupus erythematosus (SLE), rheumatoid arthritis (RA), and Sjögren's syndrome (SS), stem from a loss of immune tolerance, leading to immune-mediated damage of healthy tissues.[1-3] A cornerstone in maintaining immune homeostasis is the regulatory T cells (Treg), whose development and function critically depend on interleukin-2 (IL-2).[4] IL-2 signaling occurs through two principal receptor types: high-affinity trimeric receptors (IL-2Rα/β/γ) predominantly expressed on Tregs, and intermediate-affinity dimeric receptors (IL-2Rβ/γ) present on effector T cells (Teff) and Natural Killer (NK) cells. This difference underlies the rationale for low-dose IL-2 therapy in ADs, as it preferentially activates Tregs at low concentrations, thereby promoting immune tolerance.[5-13] Clinically, low-dose IL-2 has shown promising efficacy and safety across multiple autoimmune conditions by restoring Treg-mediated tolerance.[7,12,14,15] Nevertheless, its short serum half-life necessitates frequent administration, while its pleiotropic receptor engagement limits the extent to which systemic exposure can be increased without compromising Treg selectivity. Dose escalation may activate effector T and natural killer cells, and high-dose IL-2 therapy is associated with severe toxicities, including capillary leak syndrome, hypotension, and pulmonary edema.[16] Therefore, extending IL-2 exposure while preserving its native Treg-biased activity represents an important goal for improving low-dose IL-2 therapy.

To address these limitations, extensive protein engineering efforts have been directed toward enhancing the Treg selectivity and extending the circulating half-life of IL-2. Established strategies include chemical conjugation such as PEGylation (e.g., NKTR-214)[17,18] and the use of IL-2/anti-IL-2 antibody complexes (e.g., JES6-1).[19-22] Furthermore, extensive research is dedicated to engineering IL-2 mutants to create "superkines".[23-28] This approach utilizes rational design or directed evolution to generate variants with enhanced receptor-binding affinity and selectivity, aiming to achieve superior therapeutic potency and specificity compared to the native cytokine. While effective in improving pharmacokinetic and promoting Treg-biased activation, these approaches often rely on chemical modification or extensive sequence alteration, which can compromise intrinsic bioactivity or introduce unpredictable immune effects due to non-physiological receptor engagement.[17] Other advanced strategies have progressed clinically. For instance, the IL-2/IL-2 receptor fusion protein[29-32] (e.g., ALKS 4230, now known as Nemvaleukin alfa) is designed for selective intermediate-affinity receptor targeting and has undergone Phase III clinical trials. Similarly, "not-α" IL-2 mutants that reduce CD25 binding show potent preclinical efficacy.[33-35] However, these engineered entities frequently face similar trade-offs between stability and native function. Therefore, as a complement to established half-life extension platforms, there remains continued interest in a minimalistic yet robust engineering strategy that can substantially improve the pharmacokinetic profile of IL-2 while fully preserving its native structure and bioactivity.

In light of these challenges, chemical topology—which describes invariant spatial connectivities preserved under continuous deformation without breaking covalent bonding—offers a unique engineering avenue.[36,37] While natural proteins typically adopt linear backbones from ribosomal synthesis, recent advances leveraging genetically encoded entangling and reaction motifs have enabled the design and synthesis of diverse nonlinear protein architectures.[38-40] Over the past decade, a library of topological proteins, including cyclic, lasso, knotted, and catenated structures,[41-49] have been synthesized, demonstrating markedly enhanced proteolytic stability and prolonged plasma half-life.[50-53] The concept has been further extended to create "topological protein isoforms", which share similar 3D structures but distinct backbone topology, thereby optimizing functional performance.[48,54,55] By combining robust topological stabilization with full retention of native protein structure, this approach represents a compelling strategy to overcome the pharmacokinetic limitations of therapeutic proteins such as IL-2.

Herein, we propose protein topology engineering as an effective strategy to overcome the intrinsic pharmacokinetic limitations of IL-2. We report the design of two novel topological IL-2 variants: a cyclic form (*c*-IL-2) and a mechanically interlocked homocatenane (*cat*-IL-2). We hypothesized that such topological restructuring would confer enhanced proteolytic stability while preserving native bioactivity. Comprehensive *in vitro* and *in vivo* evaluations confirmed that both variants maintain full receptor-binding capacity and exhibit a significantly extended serum half-life relative to the wild-type IL-2.

Crucially, both molecules demonstrated potent and preferential Treg expansion, conferring durable therapeutic efficacy in multiple autoimmune disease models without eliciting detectable systemic toxicity. This work establishes protein topology engineering as a robust and minimalist platform for enhancing cytokine therapeutics, offering a promising path toward safe and long-acting, Treg-biased immunotherapy.

MATERIALS AND METHODS

DNA construction

All oligonucleotide primers were ordered from Genewiz Inc. Sequence of interleukin-2 (pET21a-IL-2) was ordered from GENEray Inc. Sequences encoding p53dim (X) and split intein were amplified by PCR from the corresponding plasmids reported in the previous work. All the genes were treated with standard restriction digestion and ligation protocols for cloning into the expression vector pET15b. All sequences of the genes above were confirmed by direct DNA sequencing.

Protein expression and purification

Plasmids containing the designed sequences were transformed into *E. coli* strain Origami (DE3) for the biosynthesis of IL-2 with different topologies. The single colony was inoculated in 5 mL of 2xYT medium with 100 μg/mL ampicillin and grew in the shaker (37°C, 250 rpm) overnight. Then the cultures were inoculated to 300 mL 2xYT medium containing 100 μg/mL ampicillin in a ratio of 1:100 and cultured at 37°C. The isopropyl β-D-1-thiogalactopyranoside (IPTG) was added to the final concentration of 0.33 mM to induce protein expression when OD_{600} reached 0.6~1 (for wt-IL-2, inducing with 0.5 mM IPTG). The cultures further grew in a shaker at 16°C for 20 h. After expression, the cells were harvested via centrifugation (6000 rpm, 15 min, 4°C). The harvested cell pellets were resuspended with 30 mL lysis buffer (50 mM NaH_2PO_4, 300 mM NaCl, 10 mM imidazole, pH=8.0) and lysed by ultrasonication. After centrifugation (12000 rpm, 45 min), the supernatant was mixed with Ni-NTA resin (GE Healthcare Inc.) and equilibrated at 4°C for 1 h. Then the resin was loaded to an empty column, washed by wash buffer 1 (50 mM NaH_2PO_4, 300 mM NaCl, 20 mM imidazole, pH=8.0) and wash buffer 2 (50 mM NaH_2PO_4, 300 mM NaCl, 50 mM imidazole, pH=8.0) for several column volumes, and then eluted by elution buffer (50 mM NaH_2PO_4, 300 mM NaCl, 250 mM imidazole, pH=8.0). The eluted products were further purified by size exclusion chromatography (SEC) performed on a Superdex 200 Increase 10/300 GL column in an ÄKTA FPLC system (GE Healthcare Inc.), with PBS buffer (137 mM NaCl, 2.7 mM KCl, 10 mM Na_2HPO_4, 2 mM KH_2PO_4, pH=7.4) as the mobile phase at a flow rate of 0.5 mL/min. Protein concentrations were determined by UV-absorbance with NanoPhotometer NP80 (Implen Inc.).

Protein characterizations

The purified protein samples were characterized by sodium dodecyl sulfate-polyacrylamide gel electrophoresis (SDS-PAGE) and SEC. 5 μL of 5 × loading buffer was added to 20 μL of each sample and heated at 98°C for 10 min before SDS-PAGE analysis. Protein samples' molecular weights were confirmed by ultra-performance liquid chromatography-mass spectrometry (LC-MS) with a quadrupole rods SQ Detector 2 mass spectrometer (Waters Corp.). MassLynx V 4.1 (Waters Corp.) was used to convert the m/z spectrum to the mass spectrum using the MaxEnt1 algorithm (Waters Corp.).

Circular dichroism (CD) spectroscopy

Protein samples were diluted with ddH_2O. The CD spectroscopy was recorded on a J-815 spectrometer (Jasco Corp.). Samples were scanned every 0.5 nm from 190 nm to 260 nm with 1 mm path length, repeating 3 times with a scanning speed of 100 nm/min.

Pharmacokinetics

The six-week-old female KM mice (Vital River Laboratories) which were randomly divided into three groups (n = 5) were injected at a dose of 60 μg IL-2/kg body weight with one of the following, wt-IL-2 (XinJier, SL PHARM), *c*-IL-2, *cat*-IL-2 (dissolved in a PBS solution) into the abdominal cavity. Peripheral blood samples (50 μL each time) were removed from orbit at selected time points below: 30 min, 1, 3, 6, 12, 24 h. The samples were allowed to stand at 4°C for four hours, followed by centrifugation at 4000 *g* for 15 min. Then, the isolated serum was stored at -80°C before analysis. A Human IL-2 ELISA kit (Neobioscience) was used to quantify the concentration of IL-2. Pharmacokinetic parameters were analyzed by GraphPad Prism software 7.0, and data were expressed as mean ± SD.

Biolayer interferometry

The BLI assays were performed at room temperature with streptavidin probes (Fortebio, Cat# 18-5020), shaking at 1000 rpm in Fortebio Octet Red 96. The samples wt-IL-2 (XinJier, SL PHARM), *c*-IL-2, and *cat*-IL-2 were diluted with running buffer (PBS, 0.05 % Tween-20, 0.5 % BSA) to 1000, 330, 110, 37 and 12 nM (IL-2). The assays were performed as steps below: (1) Sensor check: the sensors were shaken in a running buffer for 60 s. (2) Receptor loading: shaken in biotinylated human IL-2Rα or human IL-2Rβ (Biosystems, Cat# ILA-H82E6 and ILB-H82E3) at 5 μg/mL for 300 s. (3) Receptor loading check: shaken in running buffer for 60 s. (4) Association: shaken in samples at different concentrations respectively for 200 s. (5) Dissociation: shaken in running buffer (different from step 3) for 200 s. (6) Wash: shaken in washing buffer (0.1 M Glycine-HCl, pH 2.2) for 5 s, then shaking 5 s in running buffer (different from the steps 3 and 5) for 3 cycles. The kinetics and affinities data were fitted by Octet Data analysis software.

Human subjects and *in vitro* T cells assays

PBMCs were freshly isolated by centrifugation with Ficoll-Hypaque (GE Healthcare, Chicago, IL, USA). After cell count, cell concentration was adjusted to 2×10^5/mL with culture medium. Cells were added into 24-well plates and divided into four groups (PBS, wt-IL-2, *c*-IL-2, and *cat*-IL-2). Cells were collected and stained after being cultured at 37°C for 72 h. Cells were then stained with fluorescence-conjugated antibodies: FITC-conjugated anti-CD4, AlexaFluor®700-conjugated anti-CD3, Brilliant Violet 650-conjugated anti-CCR6, Brilliant Violet 421-conjugated anti-CCR7, Brilliant Violet 510-conjugated anti-CD45RA, PE-CF594-conjugated anti-CD183 (CXCR3), and AlexaFluor647-conjugated anti-CD185 (CXCR5). Multicolor flow cytometry (FACSAria II; BD Biosciences, Franklin Lakes, NJ, USA) was used to determine the proportions of T cell subsets in the periphery. Tfh was defined as $CD3^+CD4^+CD45RA^-CXCR5^+PD\text{-}1^{high}$. Circulating Tfh subsets were defined as Tfh1 ($CXCR3^+CCR6^-$), Tfh2 ($CXCR3^-CCR6^-$), or Tfh17 ($CXCR3^-CCR6^+$) among $CXCR5^+CD45RA^-CD4^+$ T cells. Furthermore, Th subsets were defined as Th1 ($CXCR3^+CCR6^-$), Th2 ($CXCR3^-CCR6^-$), or Th17 ($CXCR3^-CCR6^+$) among $CXCR5^-CD45RA^-CD4^+$ T cells. Additionally, cells were also surface-labeled with anti-CD3-PerCP, anti-CD4-FITC and anti-CD25-PE and then fixed and permeabilized with 1 mL fresh fixation/permeabilization, followed by staining with human anti-FOXP3-Alexa Fluor 647. All antibodies were obtained from BioLegend, San Diego, California. Stained cells were detected by flow cytometry (FACSAria II; BD Biosciences, Franklin Lakes, NJ, USA) and analyzed using CellQuest software. Data were analyzed using FlowJo v.5.7.2 software (Tree Star, Ashland, OR, USA). The study protocol was approved by the ethics committee of Peking University People's Hospital (2023PHB093-001).

Topological IL-2 treatment in MRL/lpr spontaneous SLE mouse model

MRL/lpr female mice were purchased from SPF Biotechnology Co., Ltd. and randomly divided into 5 groups with 6 mice in each group. The drug was injected at 12 weeks in the following way: The MRL/lpr mice were administered with wt-IL-2 (30,000 IU/mouse) three times a week for 8 weeks. Other groups were given treatments (PBS, wt-IL-2, *c*-IL-2, and *cat*-IL-2, 30,000 IU/mouse) once a week. Flow cytometry was performed on mouse spleen cells 8 weeks after drug injection, and the staining scheme is shown in Table S1. Serum of mice was collected for biochemical detection, liver, lung, heart, brain, and other tissues were collected for pathological detection. The study protocol was approved by the Institutional Ethics Committee of Peking University (2021PHE026).

Topological IL-2 treatment in the NOD mouse model

NOD mice were purchased from SPF Biotechnology Co., Ltd. and randomly divided into 4 groups with 6 mice in each group. The drug was injected at 8 weeks in the following way: The NOD mice were administered with wt-IL-2 (30,000 IU/mouse) thrice weekly for 8 weeks. Other groups were given treat-

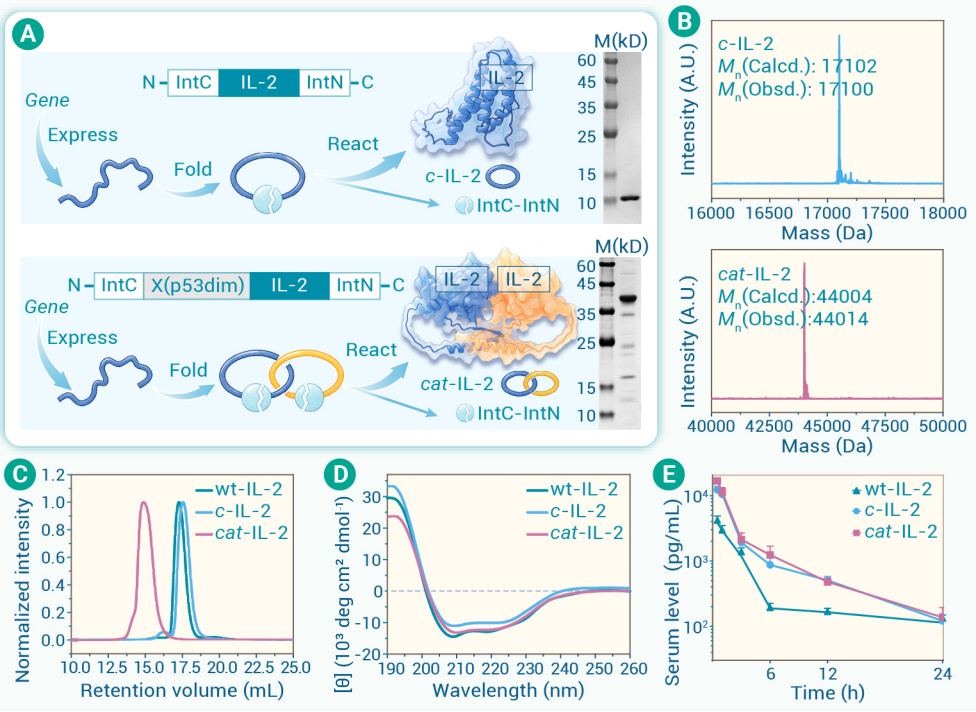


Figure 1. Cellular synthesis and biophysical characterizations of topological IL-2 variants (A) Biosynthesis of *c*-IL-2 and *cat*-IL-2. The schematic illustrates the programmed post-translational modification strategy, and the SDS-PAGE gel validates the protein products. (B) LC-MS spectra confirming the molecular identity of *c*-IL-2 and *cat*-IL-2. (C) Size exclusion chromatography (SEC) analysis of purified wt-IL-2, *c*-IL-2, and *cat*-IL-2. (D) Circular dichroism (CD) spectra demonstrating the secondary structures of wt-IL-2, *c*-IL-2, and *cat*-IL-2. (E) Pharmacokinetic profile of wt-IL-2, *c*-IL-2, and *cat*-IL-2 in KM mice. ELISA measured Serum IL-2 concentrations (pg/mL) over time following a single intraperitoneal injection. Both *c*-IL-2 and *cat*-IL-2 exhibited extended *in vivo* half-life compared to wt-IL-2.

ments (PBS, *c*-IL-2, and *cat*-IL-2, 30,000 IU/mouse) once a week. Saliva flow rate was tested for 15 minutes before and after drug injection. Flow cytometry was performed on mouse spleen and lymph node cells 8 weeks after drug injection, and the staining scheme is shown in Table S1.

Topological IL-2 treatment in the CIA mouse model

DBA/1 mice were immunized with bovine CII from CFA at day 0 and rechallenged 21 days later. The CIA mice were administered with wt-IL-2 (30,000 IU/mouse) thrice weekly for 4 weeks. Other groups were given treatments (PBS, wt-IL-2, *c*-IL-2, and *cat*-IL-2, 30,000 IU/mouse) once a week (n = 6 per group). Arthritis severity was assessed throughout the treatment period using a clinical scoring system ranging from 0 to 4 for each paw, with a maximum cumulative score of 16 per mouse. After drug injection, the mice's front and back paws were taken for pathological examination, and spleen and lymph node cells were taken for flow cytometry. The flow staining scheme is shown in Table S1.

Statistical analysis

Data are presented as the mean ± SD and were obtained using SPSS v.24.0 software. One-way ANOVA followed by Dunnett's multiple comparisons test was performed to compare all treatment against the PBS control group.

RESULTS AND DISCUSSION

Design, biosynthesis and characterization of topological IL-2 variants

Natural proteins predominantly adopt linear backbone architectures; however, topologically complex proteins such as cyclic and mechanically interlocked structures have been shown to exhibit enhanced resistance to proteolysis and improved pharmacokinetic profiles.[50-53] To exploit these functional benefits of topology engineering, we designed two IL-2 variants: a cyclic form (*c*-IL-2) with its N- and C-termini covalently linked, as exemplified in prior protein engineering studies, and a catenane form (*cat*-IL-2) with two cyclic IL-2s mechanically interlocked via p53dim (X), a dimerization domain derived from the tetramerization motif of the tumor suppressor protein p53.[41,43,45,50-52] The cyclizations were both accomplished in cells via split-intein-mediated ligation.[45,55] They represent a structurally minimalist approach to cytokine optimization, avoiding extensive mutations or laborious/bulky chemical modifications that may compromise efficacy. The wild-type IL-2 (wt-IL-2) was used as a linear control to illustrate the effects of topology. The sequence information can be found in the Supporting Information. The genes encoding these topological variants were synthesized and used to transform *Escherichia coli* Origami (DE3) cells for expression. The synergy between protein folding and split-intein-mediated ligation allows post-translational processing of nascent linear protein chains into the corresponding topological forms (Figure 1A). The resulting proteins were purified under native conditions first by Ni-NTA affinity chromatography followed by size-exclusion chromatography (SEC), without the need for refolding. Under these conditions, wt-IL-2, *c*-IL-2 and *cat*-IL-2 were all recovered as soluble proteins at low milligram-per-liter yields, which were sufficient for subsequent biochemical and functional characterization.

Both SDS-PAGE and LC-MS analyses of purified samples exhibited the expected major bands and accurate molecular masses, respectively, corresponding to the target proteins (Figures 1A-B), accompanied by minor bands arising from abortive split-intein cleavage intermediates (N-terminal/C-terminal cleavage products)[56] and side products including monocyclic species (Figure S1). The SEC analysis revealed monomodal elution profiles for all IL-2 variants (Figure 1C), with subtle shoulders: for *cat*-IL-2, the shoulder originates from non-covalently associated monocyclic species with p53-binding; for *c*-IL-2, it corresponds to intrinsic IL-2 oligomerization, a feature also observable in wild-type IL-2 but less prominent at lower yields. Notably, *c*-IL-2 displayed a slightly higher retention volume than wt-IL-2, consistent with its more compact conformation due to cyclization, while *cat*-IL-2 exhibited the lowest retention volume among them as a homodimer. To assess structural integrity, circular dichroism (CD) spectroscopy was performed. The CD spectra of both *c*-IL-2 and *cat*-IL-2 closely resembled that of wt-IL-2, displaying characteristic α-helical signatures (Figure 1D). These results indicate that neither cyclization nor catenation perturbs the secondary structure of IL-2. We next examined whether topological modifications affected the receptor-binding characteristics of IL-2. Using biolayer interferometry (BLI) on a FortéBio Octet Red 96 platform, we quantified the kinetic parameters of *c*-IL-2 and *cat*-IL-2 for IL-2Rα and IL-2Rβ subunits. Both variants exhibited binding kinetics similar to wt-IL-2,[17] with dissociation constants (K_D) in the low nanomolar range (Table 1 & Figure S2). Specifically, K_D values for IL-2Rα were 5.24×10^{-9} M for *c*-IL-2 and 4.66×10^{-9} M for *cat*-IL-2, while K_D values for IL-2Rβ were 1.20×10^{-7} M and 1.92×10^{-7} M, respectively. These data confirm the molecular integrity of these topological variants, the retention of secondary structure and receptor-binding affinity, laying the foundation for their functional equivalence to wt-IL-2.

Preferential activation and expansion of Tregs in lupus patients

To explore the immunomodulatory activity of topological IL-2 variants, we treated peripheral blood mononuclear cells (PBMCs) from SLE patients with 10 nM of wt-IL-2, *c*-IL-2, or *cat*-IL-2. Flow cytometry revealed that both *c*-IL-2 and *cat*-IL-2 robustly expanded $CD4^+CD25^+CD127^{low}$ Tregs (Figure 2A), similar to wt-IL-2. Importantly, phosphorylated STAT5 (pSTAT5) levels were significantly elevated in $CD4^+$ T cells with no significant difference observed in pSTAT5 induction between wt-IL-2 and the topological IL-2 variants under the tested conditions, indicating intact downstream signaling (Figure 2F). In addition, treatment with topological IL-2 modestly changed the frequencies

Table 1. The kinetic parameters and affinities for IL-2 and its topological variants binding to IL-2R.

Variants	Receptor	K_{on} ($M^{-1}·s^{-1}$)	K_{off} (s^{-1})	K_D (M)
wt-IL-2	IL-2Rα	(2.13 ± 0.10) × 10^6	(6.66 ± 0.07) × 10^{-3}	(3.13 ± 0.15) × 10^{-9}
c-IL-2	IL-2Rα	(5.13 ± 0.18) × 10^5	(2.69 ± 0.06) × 10^{-3}	(5.24 ± 0.21) × 10^{-9}
cat-IL-2	IL-2Rα	(2.96 ± 0.03) × 10^5	(1.38 ± 0.02) × 10^{-3}	(4.66 ± 0.08) × 10^{-9}
wt-IL-2	IL-2Rβ	(2.05 ± 0.05) × 10^4	(3.06 ± 0.05) × 10^{-3}	(1.49 ± 0.04) × 10^{-7}
c-IL-2	IL-2Rβ	(2.55 ± 0.13) × 10^4	(3.07 ± 0.04) × 10^{-3}	(1.20 ± 0.06) × 10^{-7}
cat-IL-2	IL-2Rβ	(1.25 ± 0.03) × 10^4	(2.41 ± 0.04) × 10^{-3}	(1.92 ± 0.06) × 10^{-7}

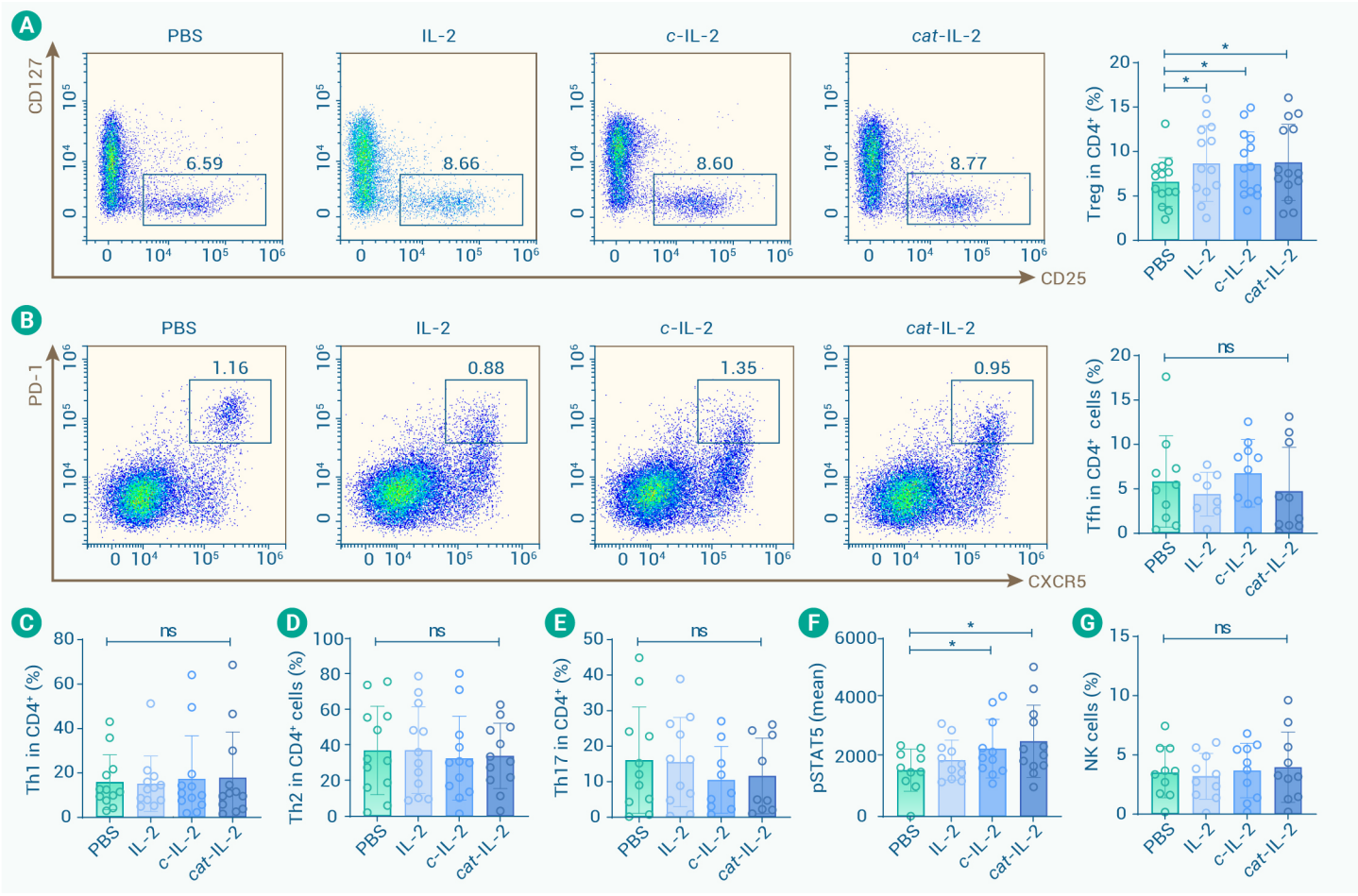


Figure 2. Immunomodulatory effects of topological IL-2 variants on Treg and Teff cell balance in SLE (A–B) Representative flow cytometry plots and quantitative analysis of Treg and Tfh cells following IL-2 treatment of PBMCs from SLE patients. PBMCs isolated from SLE patients were stimulated with each topological IL-2 variant for 72 h. (C–E) Proportions of Th1, Th2, and Th17 cells in response to *in vitro* stimulation with topological IL-2 variants. (F) Enhanced STAT5 phosphorylation in $CD4^+$ T cells following 15 min stimulation with IL-2 variants, as measured by intracellular flow cytometry. (G) Alterations in NK cell populations upon IL-2 stimulation. (n=12)

of T follicular helper (Tfh) and Th17 cells under the culture conditions tested, though statistical significance was not achieved (Figures 2B–E). The dedicated differentiation assays would be required to address this question mechanistically. Natural killer (NK) cell populations remained unchanged (Figure 2G), supporting the preferential Treg-enriching action of these IL-2 variants. These data suggest that topological IL-2 can restore the Treg/Teff balance in autoimmune conditions. However, systematic investigations into other distinct immune compartments, particularly $CD8^+$ T cells and B cells, are warranted in future studies to fully delineate this preferential activity.

To shed light on the underlying mechanisms, we investigated the transcriptional impact of topological IL-2 variants on $CD4^+$ T cell subsets. We isolated $CD4^+$ T cells from the peripheral blood of SLE patients and cultured them *in vitro* with wt-IL-2, *c*-IL-2, and *cat*-IL-2 for 4 days. RNA sequencing (RNA-seq) was then performed to evaluate gene expression changes associated with Treg and conventional T helper (Tconv) cell differentiation. Given the 4-day culture period, these transcriptomic data primarily reflect later-stage effects influenced by cell survival, proliferation, and compositional changes, rather than early proximal signaling events.[57] This aligns with prior work demonstrating that prolonged IL-2 stimulation (e.g., 72 h and beyond) drives broad proliferative and metabolic remodeling.

To explore the underlying molecular mechanisms, we evaluated the transcriptomic profiles of $CD4^+$ T cells following treatment. As shown in the targeted heatmap of selected immune-related genes (Figure 3A) and the global hierarchical clustering (Figure S3D), all IL-2 forms induced transcriptional signatures consistent with immunoregulatory activity, which was further supported by volcano plot analyses (Figures S3A-C & S4). Interestingly, the Venn diagram illustrating differentially expressed genes (DEGs) for each treatment group relative to the PBS control revealed that the overlap among the three IL-2 groups was limited to only 4.91% (Figure 3B), suggesting that *c*-IL-2 and *cat*-IL-2 induce partially distinct transcriptional programs

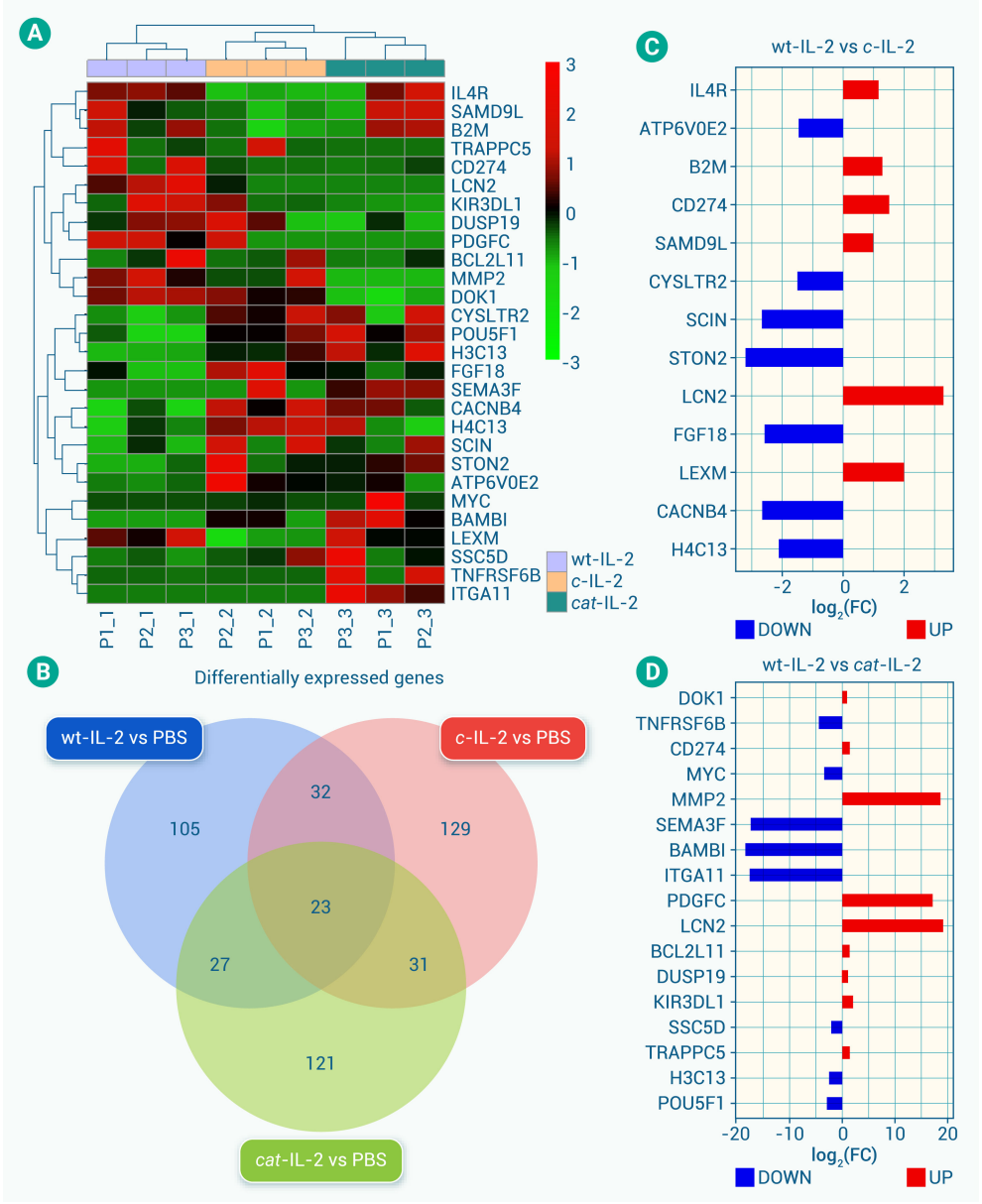


Figure 3. Transcriptomic analysis of CD4⁺T cells in response to IL-2 treatment (A) Heatmap of selected immune-related genes (up-regulated in red, down-regulated in green). (B) Venn diagram showing overlap of DEGs among wt-IL-2, *c*-IL-2, and *cat*-IL-2 treatment groups relative to the PBS control. (C–D) Distribution of up- and down-regulated signature genes in response to wt-IL-2 vs. *topo*-IL-2. RNA-seq was conducted on sorted CD4⁺ T cells from lupus patients (n = 3).

Table 2. Pharmacokinetic parameters of wt-IL-2 and its topological variants.

Samples (i.p.)	$t_{1/2}$ (α) h	$t_{1/2}$ (β) h	$AUC_{0-\infty}$ ng·h·mL^{-1}	T_{max} h	C_{max} ng·mL^{-1}	Cl/F mL·kg^{-1}·h^{-1}
wt-IL-2	NA	1.25 ± 0.11	15.55 ± 0.93	≤ 0.5	3.8 ± 0.9	3858.0 ± 232.8
c-IL-2	0.90 ± 0.10	6.23 ± 0.49	35.61 ± 1.89	≤ 0.5	12.2 ± 1.5	1684.8 ± 89.6
cat-IL-2	0.83 ± 0.01	5.67 ± 0.49	40.79 ± 3.01	≤ 0.5	16.8 ± 3.8	1470.8 ± 109.2

C_{max} (maximum drug concentration); T_{max} (time of maximal drug concentration); Cl/F (apparent clearance); i.p. (intraperitoneally). Data are mean ± SD (n=5), shown in Figure 1E.

from wt-IL-2 under prolonged treatment.

Comparative DEG analysis between topological IL-2 variants and wt-IL-2 (Figures 3A & S3E) revealed that several immune activation genes—including IL4R, CD274 (PD-L1), B2M, and LCN2—were significantly downregulated in cells treated with *c*-IL-2 and *cat*-IL-2 (Figures 3C–D). Pathway enrichment analysis confirmed that these downregulated genes were primarily associated with antigen presentation, T cell costimulation, and inflammatory cytokine signaling (Figure S4). This suggests that topological IL-2 confers a more tolerogenic and less inflammatory transcriptional profile than wt-IL-2. They not only promote Treg differentiation but also repress effector T cell activation at the transcriptomic level, thereby contributing to the restoration of immune homeostasis in SLE.

Topological IL-2 variants improve immune regulation and disease outcomes in the MRL/lpr lupus model with favorable safety profiles

To assess the pharmacokinetic profiles of topological IL-2 variants, we investigated their serum half-life in female KM mice. Mice received a single intraperitoneal injection of wt-IL-2, *c*-IL-2, and *cat*-IL-2, and the IL-2 concentrations in peripheral blood were monitored over time. As shown in Table 2 & Figure 1E, both *c*-IL-2 and *cat*-IL-2 displayed markedly prolonged half-lives compared to wt-IL-2. The β-phase elimination half-life for *c*-IL-2 was 6.23 h and for *cat*-IL-2 was 5.67 h, in contrast to 1.25 h for wt-IL-2. The ~5-fold extension in half-life and the unperturbed IL-2 receptor-binding interface ensures selective engagement with trimeric IL-2 receptors on Tregs. Moreover, the enhanced stability also translated into higher area under the curve (AUC) values and lower plasma clearance (Cl), indicating improved systemic exposure and reduced dosing demands. These findings demonstrate that topology engineering significantly enhances the pharmacokinetic profiles of IL-2 without requiring chemical conjugation or special formulation.

Encouraged by this result, we proceeded to evaluate the therapeutic efficacy of topological IL-2 variants in the MRL/lpr mouse model of SLE, especially at prolonged dosing intervals. We first optimized the dosing schedules for each IL-2 formulation based on the above pharmacokinetic analyses, tailored to fit the low-dose IL-2 therapy. wt-IL-2 was administered subcutaneously thrice weekly, whereas *c*-IL-2 and *cat*-IL-2 were administered once weekly due to their extended half-lives. Female MRL/lpr mice were treated from 12 to 20 weeks of age (Figure 4A). Treatment with all IL-2 variants led to a significant increase in the frequency and absolute number of splenic CD4⁺CD25⁺FOXP3⁺ regulatory T cells (Tregs) and reductions in proinflammatory follicular helper T (Tfh) and Th17 cells (Figures 4B–C, H–I & S5A–C). These immunomodulatory effects were most pronounced in the *cat*-IL-2 group. Correspondingly, the topological IL-2 variants exhibited significant decreases in primary disease activity metrics. Compared to PBS-treated controls, the IL-2 treated groups showed decreased proteinuria (Figure 4G), lower visceral index scores (Figures 4D & J), and significantly improved skin lesion scores (Figures 4E & K). Notably, histopathological analysis of renal tissue revealed that both *c*-IL-2 and *cat*-IL-2 significantly mitigated renal damage (Figure 4F). As exploratory endpoints, we further evaluated the impact of topological IL-2 on B cell responses and autoantibody production. We observed a statistically significant reduction in splenic B220⁺CD4⁻CD95⁺GL7⁺ germinal center B (GCB) cells following topo-

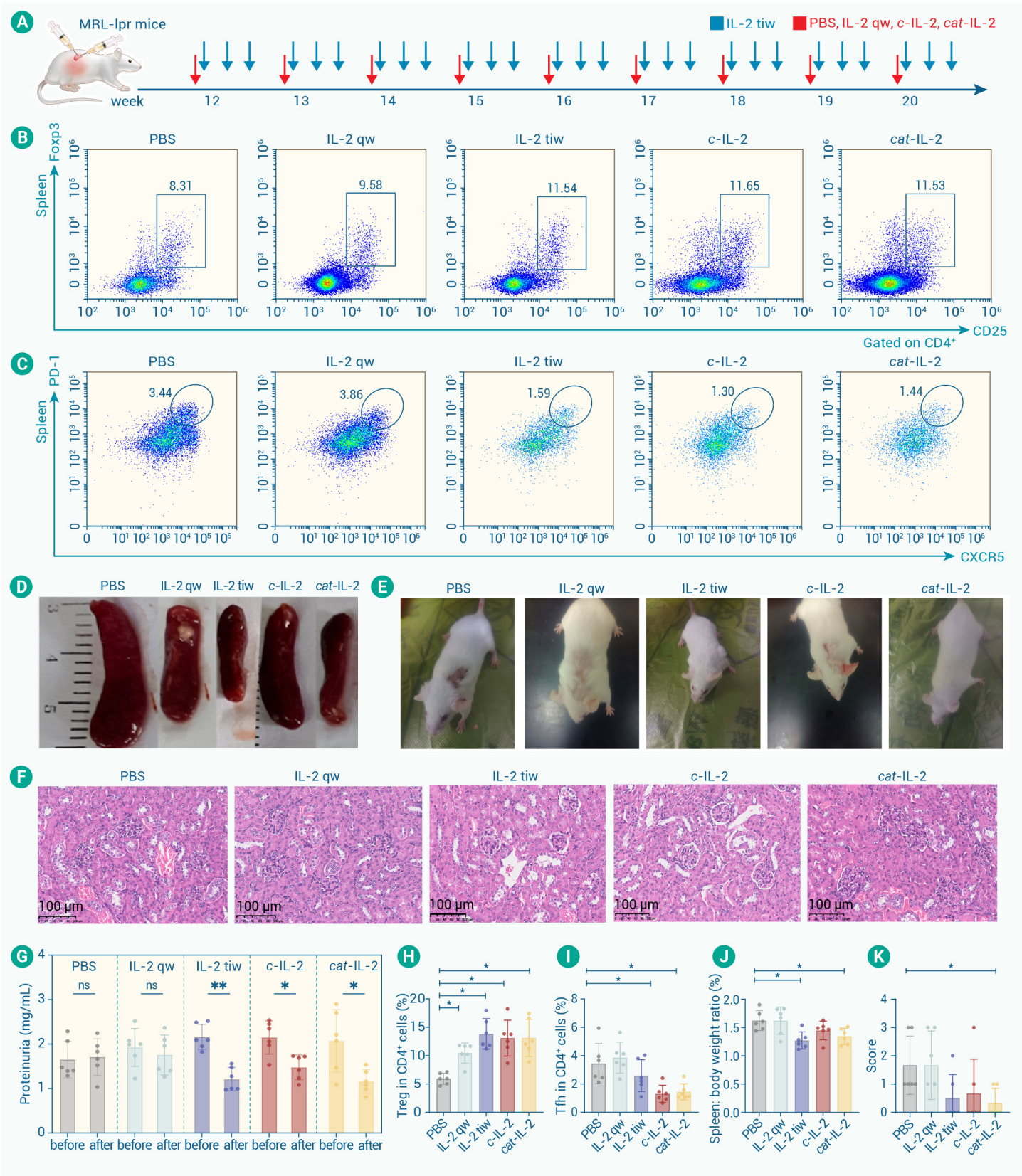


Figure 4. Therapeutic efficacy of half-life-extended IL-2 variants in MRL/lpr lupus-prone mice (A) Treatment schedule: wt-IL-2 (IL-2 tiw) administered thrice weekly; PBS, wt-IL-2 (IL-2 qw), *c*-IL-2 and *cat*-IL-2 administered weekly. (B–C) & (H–I) Flow cytometry analysis of Treg and Tfh cell frequencies post-treatment in spleen following the indicated treatments. (D & J) Comparison of spleen-to-body weight ratio among groups. (E & K) Skin lesion score of MRL/lpr mice. Skin severity was scored blinded on a 0–4 scale based on erythema, scaling, and alopecia. (F) Renal histopathology after IL-2 treatment. (G) The improvement of proteinuria after different treatment. Urinary protein levels (mg/ml) were measured before and after treatment using an ELISA assay. All experiments were performed using female MRL/lpr mice (n = 6 per group) Tiw: three times per week, qw: once weekly.

logical-IL-2 treatment (Figure S5D). Furthermore, we assessed serum levels of anti-double-stranded DNA (anti-dsDNA) and antinuclear antibodies (ANA) (Figures S5E–G). While the *cat*-IL-2 group showed a trend toward reduced autoantibody levels, these reductions were not uniformly significant across all

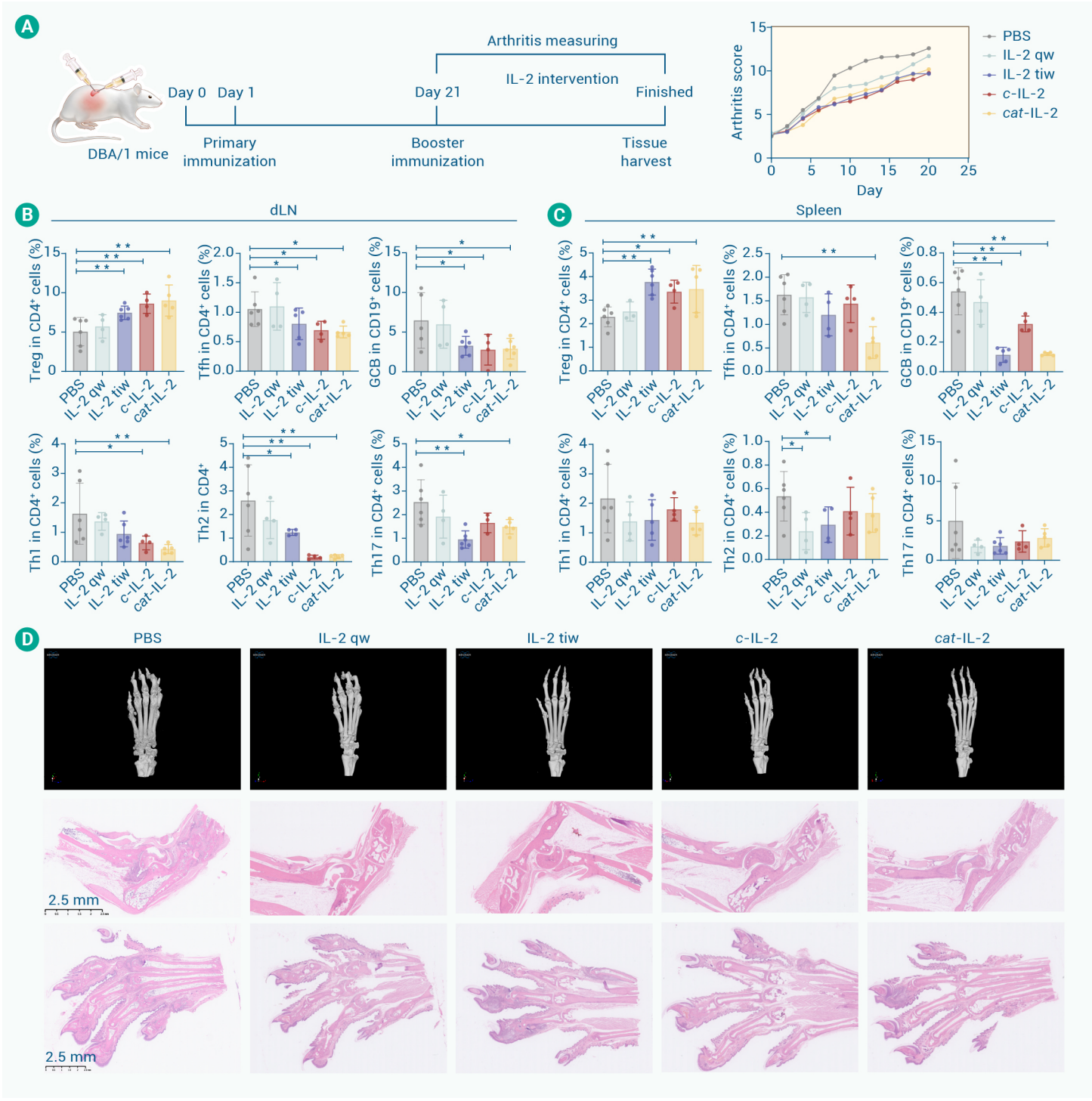


Figure 5. Efficacy of topological IL-2 variants therapy in CIA mouse (A) The experimental design for 4 weeks of IL-2 treatment using the classic CIA mouse model of RA. DBA/1 mice were immunized with bovine CII from CFA at day 0 and rechallenged 21 days later. The mice were administrated with wt-IL-2 thrice weekly for 4 weeks. Other groups were given treatments (PBS, wt-IL-2, *c*-IL-2, and *cat*-IL-2) once a week. Arthritis scores in CIA mice with wt-IL-2 and topological IL-2 variants therapy. The scoring continued with processing and was scored on a scale of 0 to 4 for each leg, with a cumulative score of 0 to 16 for each mouse. (B–C) The frequency of Treg cells ($CD4^+CD25^+Foxp3^+$), Tfh cells ($CD4^+PD\text{-}1^+CXCR5^+$), GC B cells ($B220^+GL\text{-}7^+CD95^+$), Th1 cells ($CD4^+IFN\gamma^+$), Th2 ($CD4^+IL4^+$), and Th17($CD4^+IL17^+$) in lymph node (dLN) and spleen. (D) Arthritis and bone erosion of the paws by images of micro-CT, and hematoxylin and eosin (H&E) staining. (n = 6 per group)

IL-2 treatment groups when compared to the PBS control. These findings suggest that the robust therapeutic benefits observed in this model may be driven predominantly by Treg-mediated cellular modulation and direct tissue protection, rather than acute systemic autoantibody clearance.

High-dose IL-2 therapy is associated with toxicities such as vascular leak syndrome, liver dysfunction, and neurological disorders.[16] Given the immunomodulatory preference and extended half-life of topological IL-2 variants, we further evaluated their safety profile in the MRL/lpr lupus model. Histopathological examination of lung, liver, and cardiac tissues via hematoxylin and eosin (H&E) staining revealed no signs of pulmonary edema, inflammatory infiltrates, or vascular leak syndrome in mice treated with *c*-IL-2 or *cat*-IL-2 (Figure S6A). Serum biochemical markers, such as urea, glucose (GLU), alanine aminotransferase (ALT), and aspartate aminotransferase (AST), remained within normal physiological ranges across all treatment groups (Figures S6B–G). Thus, despite their sustained bioactivity, topological IL-2 variants did not elicit systemic toxicity, pulmonary edema or tissue damage in autoimmune-prone MRL/lpr mice. These findings highlight a favorable safety profile for topological IL-2 variants, particularly *cat*-IL-2,

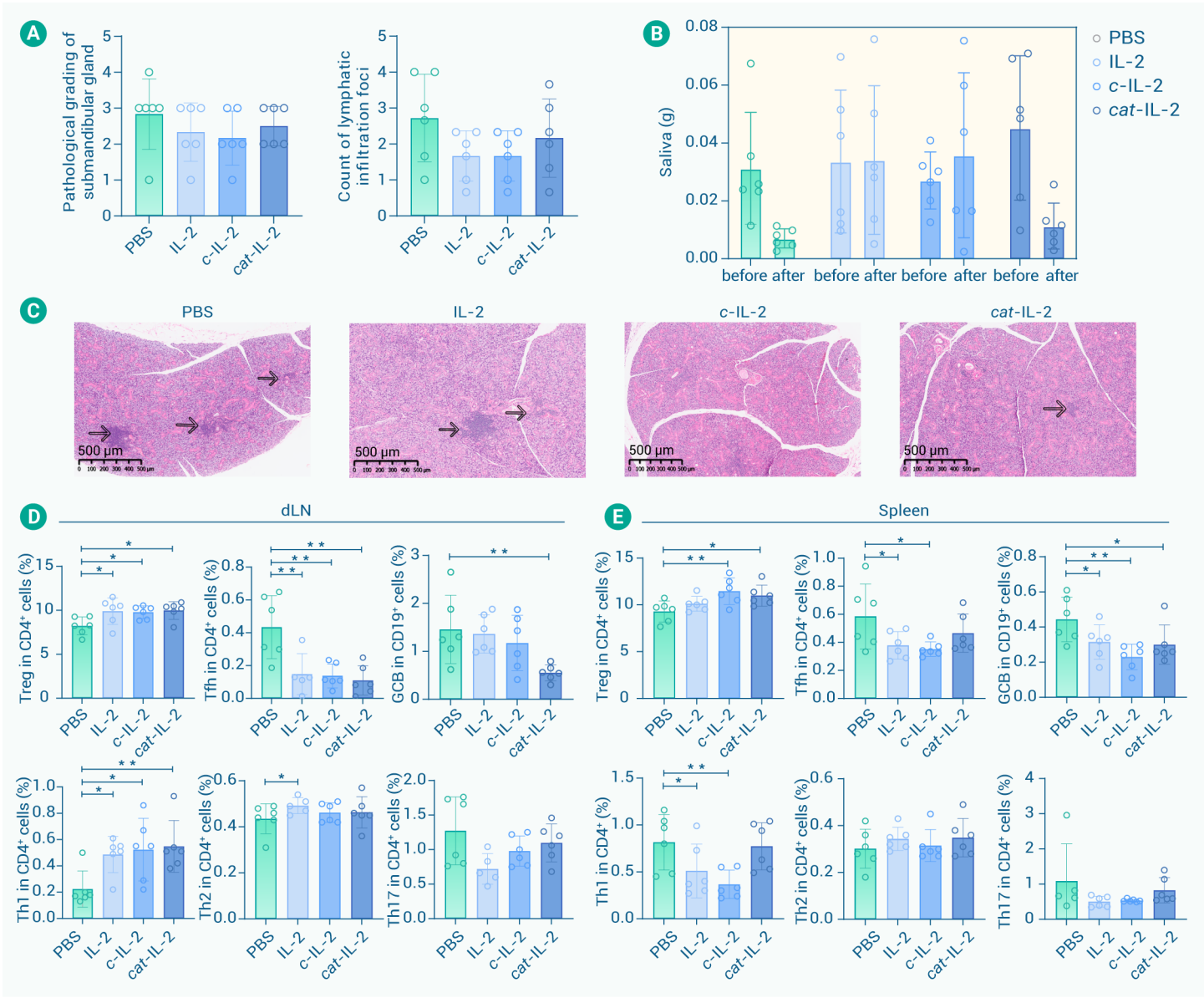


Figure 6. Efficacy of topological IL-2 variants therapy in SS mouse model-NOD (A) Submandibular gland histological grading and lymphocyte infiltration foci count of NOD mice after IL-2 administration. (B) Comparisons of the salivary flow rate before and after treatment in 15 minutes. (C) Submandibular gland pathology of NOD mice after wt-IL-2 and topological IL-2 variants treatment. (D–E) Flow cytometry analysis revealing the frequency of Treg cells ($CD4^+CD25^+Foxp3^+$), Tfh cells ($CD4^+PD\text{-}1^+CXCR5^+$), GC B cells ($B220^+GL\text{-}7^+CD95^+$), Th1 cells ($CD4^+IFN\gamma^+$), Th2 ($CD4^+IL4^+$), and Th17($CD4^+IL17^+$) in lymph node and spleen. (n = 6 per group)

alongside their potent immunomodulatory and disease-ameliorating effects in SLE. The absence of liver toxicity, as indicated by stable ALT and AST levels, suggests a broader therapeutic window suitable for chronic autoimmune indications. Moreover, emerging evidence indicates that IL-2 signaling can engage lymphoid dendritic cell pathways to enhance antitumor immunity, further underscoring the therapeutic promise of these safer IL-2–based agents.[58-61]

Efficacy of topological IL-2 therapy in other autoimmune diseases.

To evaluate the broader therapeutic applicability of topological IL-2 variants, we also examined their effects in rheumatoid arthritis and Sjögren's syndrome. In an initial *in vitro* assessment, PBMCs from patients with RA and SS were cultured with wt-IL-2, *c*-IL-2, or *cat*-IL-2. All IL-2 forms increased the proportion of Tregs, confirming their ability to promote Treg expansion across autoimmune conditions (Figure S7). Then, we used the collagen-induced arthritis (CIA) mouse model to assess *in vivo* efficacy in RA. Using the same dosing regimen established in prior studies (Figure 5A),[62] both *c*-IL-2 and *cat*-IL-2 significantly increased Treg frequencies in the spleen and draining lymph nodes (DLNs). This immunomodulatory shift was associated with a reduced incidence of arthritis, decreased joint swelling, and attenuated bone erosion, as observed by clinical scoring and histological analysis (Figures 5B–D). Similarly, we also treated non-obese diabetic (NOD) mice—a spontaneous SS-like model—with either wt-IL-2 (30,000 IU/mouse) thrice weekly or topological IL-2 (30,000 IU/week) from 8 to 16 weeks of age (Figure 6). By week 16, mice receiving *c*-IL-2 exhibited reduced salivary gland inflammation, preserved glandular structure, and improved secretory function compared to both PBS and wt-IL-2 groups (Figures 6A–C). The weaker local efficacy of *cat*-IL-2 might stem from its larger hydrodynamic radius, which restricts its penetration into the dense submandibular gland. Flow cytometry revealed increased Tregs and decreased $B220^+GL\text{-}7^+CD95^+$ germinal center B cells in both spleens and submandibular draining lymph nodes (Figures 6D–E). Histopathological scoring, performed blindly by an independent pathologist, confirmed a lower inflammatory score in topologically IL-2 treated animals. Together, these findings demonstrate that topological IL-2 variants, particularly *cat*-IL-2, are effective in modulating immune homeostasis and ameliorating disease phenotypes across multiple autoimmune conditions. While this universal efficacy is primarily driven by robust Treg expansion, the concomitant reductions in GC B and Tfh cells likely represent secondary immunological changes whose mechanistic contributions vary depending on the specific disease context. For instance, because disease

pathogenesis in the MRL/lpr model is primarily driven by extrafollicular B cell responses rather than the classical GC/Tfh axis,[63] the observed decreases in Tfh and GC B cells in this model should be explicitly interpreted as associated consequences of a rebalanced immune environment, rather than the primary mechanism of therapeutic efficacy. The consistent therapeutic benefit across distinct autoimmune models toward restoration of immune regulation highlights the generalizability of this approach.

Despite these promising findings, several limitations should be acknowledged. First, the scope of this study was limited to autoimmune disease models; the utility of topological IL-2 in cancer or infectious diseases remains to be determined. Second, although we primarily focused on Tregs, various studies also reported that low-dose IL-2 can modulate $CD8^+$ T cells to enhance antiviral immunity,[64,65] further studies are warranted to assess the impact of these variants on other immune compartments, including NK cells, $CD8^+$ T cells, and B cells. Third, optimal dosing regimens and injection intervals were not fully explored and merit further pharmacodynamic investigation. Additionally, a sequence-matched linear control was not included, as the inherent instability of uncyclized precursors precludes fully decoupling sequence effects from topological constraints. Lastly, although the current study revealed no overt toxicity in the tested mouse models and we anticipate the introduced exogenous components (e.g., split-intein remnant linkers and the p53dim motif) to be biologically inert, their precise in vivo roles remain to be fully elucidated, necessitating dedicated future studies to systematically evaluate anti-drug antibody formation, repeat-dose immunogenicity, pharmacokinetic neutralization, and immune-complex-related safety risks for successful translational development. Nonetheless, the clinical value of this minimalist approach should not be underestimated, not to mention that they can be used in conjugation with other protein engineering techniques to further enhance their performances.

CONCLUSION

In summary, we present a proof-of-concept study of using protein topology engineering as a next-generation strategy to optimize cytokine therapies. The development of *c*-IL-2 and *cat*-IL-2 provides a compelling platform for long-acting, Treg-favoring immunomodulation with broad translational potential in autoimmune diseases. A key finding is that *c*-IL-2 and *cat*-IL-2 exhibit immune-regulatory effects *in vitro*, preferentially driving the activation and expansion of Tregs. This Treg bias is particularly significant in SLE, where restoring Treg homeostasis is essential for durable disease control.[9,66] Both variants promoted FOXP3 expression and STAT5 phosphorylation while suppressing proinflammatory T helper 17 (Th17) and follicular helper T (Tfh) cell subsets. RNA-seq analysis further revealed the induction of tolerogenic transcriptional profiles following sustained exposure, indicating a systemic shift toward immune tolerance. These immunomodulatory effects suggest broader therapeutic applicability beyond SLE. Hence, they were further assessed in three well-established models of autoimmunity: MRL/lpr (SLE), collagen-induced arthritis (CIA), and non-obese diabetic (NOD) mice. In all models, both *c*-IL-2 and *cat*-IL-2 significantly ameliorated core clinical manifestations, including reductions in proteinuria, skin lesions, tissue damage and lymphoid infiltration. This minimalist engineering approach achieves enhanced pharmacological performance while preserving the native function of IL-2, opening new avenues for precision immune intervention. We believe that this approach should also be applicable to other cytokines as well, giving rise to a new class of topological cytokine therapies.

REFERENCES

1. Franklyn K., Hoi A., Nikpour M., et al. (2014). The need to define treatment goals for systemic lupus erythematosus. *Nat. Rev. Rheumatol.* **10**:567–571. DOI:10.1038/nrrheum.2014.118
2. Ugarte-Gil M. F., Wojdyla D., Pons-Estel G. J., et al. (2017). Remission and Low Disease Activity Status (LDAS) protect lupus patients from damage occurrence: Data from a multiethnic, multinational Latin American Lupus Cohort (GLADEL). *Ann. Rheum. Dis.* **76**:2071–2074. DOI:10.1136/annrheumdis-2017-211814
3. Morand E. F. and Mosca M. (2017). Treat to target, remission and low disease activity in SLE. *Best Pract. Res. Clin. Rheumatol.* **31**:342–350. DOI:10.1016/j.berh.2017.09.009
4. Boyman O. and Sprent J. (2012). The role of interleukin-2 during homeostasis and activation of the immune system. *Nat. Rev. Immunol.* **12**:180–190. DOI:10.1038/nri3156
5. Koreth J., Matsuoka K., Kim H. T., et al. (2011). Interleukin-2 and regulatory T cells in graft-versus-host disease. *N. Engl. J. Med.* **365**:2055–2066. DOI:10.1056/NEJMoa1108188
6. Saadoun D., Rosenzwajg M., Joly F., et al. (2011). Regulatory T-cell responses to low-dose interleukin-2 in HCV-induced vasculitis. *N. Engl. J. Med.* **365**:2067–2077. DOI:10.1056/NEJMoa1105143
7. Mizui M. and Tsokos G. C. (2016). Low-dose IL-2 in the treatment of lupus. *Curr. Rheumatol. Rep.* **18**:68. DOI:10.1007/s11926-016-0617-5
8. Kim N., Jeon Y. W., Nam Y. S., et al. (2016). Therapeutic potential of low-dose IL-2 in a chronic GVHD patient by in vivo expansion of regulatory T cells. *Cytokine* **78**:22–26. DOI:10.1016/j.cyto.2015.11.020
9. He J., Zhang X., Wei Y., et al. (2016). Low-dose interleukin-2 treatment selectively modulates CD4(+) T cell subsets in patients with systemic lupus erythematosus. *Nat. Med.* **22**:991–993. DOI:10.1038/nm.4148
10. Dwyer C. J., Ward N. C., Pugliese A., et al. (2016). Promoting immune regulation in type 1 diabetes using low-dose interleukin-2. *Curr. Diab. Rep.* **16**:46. DOI:10.1007/s11892-016-0739-1
11. Rosenzwajg M., Lorenzon R., Cacoub P., et al. (2019). Immunological and clinical effects of low-dose interleukin-2 across 11 autoimmune diseases in a single, open clinical trial. *Ann. Rheum. Dis.* **78**:209–217. DOI:10.1136/annrheumdis-2018-214229
12. He J., Zhang R., Shao M., et al. (2020). Efficacy and safety of low-dose IL-2 in the treatment of systemic lupus erythematosus: A randomised, double-blind, placebo-controlled trial. *Ann. Rheum. Dis* **79**:141–149. DOI:10.1136/annrheumdis-2019-215396
13. Li Z. G., He J., Miao M. (2023). Low-dose interleukin-2 therapy in autoimmune and inflammatory diseases: Facts and hopes. *Sci. Bull.* **68**:10–13. DOI:10.1016/j.scib.2022.12.024
14. von Spee-Mayer C., Siegert E., Abdirama D., et al. (2016). Low-dose interleukin-2 selectively corrects regulatory T cell defects in patients with systemic lupus erythematosus. *Ann. Rheum. Dis.* **75**:1407–1415. DOI:10.1136/annrheumdis-2015-207776
15. Miao M., Xiao X., Tian J., et al. (2021). Therapeutic potential of targeting Tfr/Tfh cell balance by low-dose-IL-2 in active SLE: A post hoc analysis from a double-blind RCT study. *Arthritis Res. Ther.* **23**:167. DOI:10.1186/s13075-021-02535-6
16. Shah N. R., Declouette B., Ansari-Gilani K., et al. (2021). High-dose interleukin-2 therapy related adverse events and implications on imaging. *Diagn. Interv. Radiol.* **27**:684–689. DOI:10.5152/dir.2021.20503
17. Zhang B., Sun J., Wang Y., et al. (2021). Site-specific PEGylation of interleukin-2 enhances immunosuppression via the sustained activation of regulatory T cells. *Nat. Biomed. Eng.* **5**:1288–1305. DOI:10.1038/s41551-021-00797-8
18. Tannir N. M., Formiga M. N., Penkov K., et al. (2024). Bempegaldesleukin plus nivolumab versus sunitinib or cabozantinib in previously untreated advanced clear cell renal cell carcinoma: A phase III randomized study (PIVOT-09). *J. Clin. Oncol.* **42**:2800–2811. DOI:10.1200/JCO.23.02082
19. Trotta E., Bessette P. H., Silveria S. L., et al. (2018). A human anti-IL-2 antibody that potentiates regulatory T cells by a structure-based mechanism. *Nat. Med.* **24**:1005–1014. DOI:10.1038/s41591-018-0070-2
20. Spangler J. B., Trotta E., Tomala J., et al. (2018). Engineering a single-agent cytokine/antibody fusion that selectively expands regulatory T cells for autoimmune disease therapy. *J. Immunol.* **201**:2094–2106. DOI:10.4049/jimmunol.1800578
21. Lee J. Y., Lee E., Hong S. W., et al. (2020). TCB2, a new anti-human interleukin-2 antibody, facilitates heterodimeric IL-2 receptor signaling and improves anti-tumor immunity. *Oncoimmunology* **9**:1681869. DOI:10.1080/2162402x.2019.1681869
22. Karakus U., Sahin D., Mittl P. R. E., et al. (2020). Receptor-gated IL-2 delivery by an anti-human IL-2 antibody activates regulatory T cells in three different species. *Sci. Transl. Med.* **12**:eabb9283. DOI:10.1126/scitranslmed.abb9283
23. Liu D. V., Maier L. M., Hafler D. A., et al. (2009). Engineered interleukin-2 antagonists for the inhibition of regulatory T cells. *J. Immunother.* **32**:887–894. DOI:10.1097/CJI.0b013e3181b528da
24. Levin A. M., Bates D. L., Ring A. M., et al. (2012). Exploiting a natural conformational switch to engineer an interleukin-2 'superkine'. *Nature* **484**:529–533. DOI:10.1038/nature10975
25. Carmenate T., Pacios A., Enamorado M., et al. (2013). Human IL-2 mutein with higher antitumor efficacy than wild type IL-2. *J. Immunol.* **190**:6230–6238. DOI:10.4049/jimmunol.1201895
26. Mitra S., Ring A. M., Amarnath S., et al. (2015). Interleukin-2 activity can be fine tuned with engineered receptor signaling clamps. *Immunity* **42**:826–838. DOI:10.1016/j.immuni.2015.04.018
27. Sockolosky J. T., Trotta E., Parisi G., et al. (2018). Selective targeting of engineered T cells using orthogonal IL-2 cytokine-receptor complexes. *Science* **359**:1037–1042. DOI:10.1126/science.aar3246
28. Carmenate T., Ortíz Y., Enamorado M., et al. (2018). Blocking IL-2 signal in vivo with an IL-2 antagonist reduces tumor growth through the control of regulatory T cells. *J. Immunol.* **200**:3475–3484. DOI:10.4049/jimmunol.1700433
29. Ward N. C., Yu A., Moro A., et al. (2018). IL-2/CD25: A long-acting fusion protein that promotes immune tolerance by selectively targeting the IL-2 receptor on regulatory T cells. *J. Immunol.* **201**:2579–2592. DOI:10.4049/jimmunol.1800907

30. Lopes J. E., Fisher J. L., Flick H. L., et al. (2020). ALKS 4230: A novel engineered IL-2 fusion protein with an improved cellular selectivity profile for cancer immunotherapy. *J. Immunother. Cancer* **8**:e000673. DOI:10.1136/jitc-2020-000673
31. Zhang B., Sun J., Yuan Y., et al. (2023). Proximity-enabled covalent binding of IL-2 to IL-2Rα selectively activates regulatory T cells and suppresses autoimmunity. *Signal Transduct. Target. Ther.* **8**:28. DOI:10.1038/s41392-022-01208-3
32. Vaishampayan U. N., Muzaffar J., Winer I., et al. (2024). Nemvaleukin alfa, a modified interleukin-2 cytokine, as monotherapy and with pembrolizumab in patients with advanced solid tumors (ARTISTRY-1). *J. Immunother. Cancer* **12**:e010143. DOI:10.1136/jitc-2024-010143
33. Kobayashi M., Kojima K., Murayama K., et al. (2021). MK-6, a novel not-alpha IL-2, elicits a potent antitumor activity by improving the effector to regulatory T cell balance. *Cancer Sci.* **112**:4478–4489. DOI:10.1111/cas.15127
34. Moynihan K. D., Kumar M. P., Sultan H., et al. (2024). IL2 targeted to CD8+ T cells promotes robust effector T-cell responses and potent antitumor immunity. *Cancer Discov.* **14**:1206–1225. DOI:10.1158/2159-8290.CD-23-1266
35. Sun J., Guo L., Ji D., et al. (2025). Reshape the fates of Treg and CD8+ T cells through IL-2Ralpha by synergizing divergent receptor-biased IL-2 PEGylates. *Adv. Sci.* **12**:e2414931. DOI:10.1002/advs.202414931
36. Francl M. (2009). Stretching topology. *Nat. Chem.* **1**:334–335. DOI:10.1038/nchem.302
37. Wang X.-W. and Zhang W.-B. (2018). Chemical topology and complexity of protein architectures. *Trends Biochem. Sci.* **43**:806–817. DOI:10.1016/j.tibs.2018.07.001
38. Qu Z., Cheng S. Z. D., Zhang W.-B. (2021). Macromolecular topology engineering. *Trends Chem.* **3**:402–415. DOI:10.1016/j.trechm.2021.02.002
39. Li T., Zhang F., Fang J., et al. (2023). Rational design and cellular synthesis of proteins with unconventional chemical topology. *Chin. J. Chem.* **41**:2873–2880. DOI:10.1002/cjoc.202300190
40. Wang Y.-X., Wu W.-H., Jiang F.-Y., et al. (2024). Mechanically interlocked biomacromolecules. *Supramol. Mater.* **3**:100059. DOI:10.1016/j.supmat.2023.100059
41. Yan L. Z. and Dawson P. E. (2001). Design and synthesis of a protein catenane. *Angew. Chem. Int. Ed.* **40**:3625–3627. DOI:10.1002/1521-3773(20011001)40:19<3625::AID-ANIE3625>3.0.CO;2-Q
42. King N. P., Jacobitz A. W., Sawaya M. R., et al. (2010). Structure and folding of a designed knotted protein. *Proc. Natl. Acad. Sci. USA* **107**:20732–20737. DOI:10.1073/pnas.1007602107
43. Wang X.-W. and Zhang W.-B. (2016). Cellular synthesis of protein catenanes. *Angew. Chem. Int. Ed.* **55**:3442–3446. DOI:10.1002/anie.201511640
44. Liu Y., Wu W.-H., Hong S., et al. (2020). Lasso proteins: Modular design, cellular synthesis, and topological transformation. *Angew. Chem. Int. Ed.* **59**:19153–19161. DOI:10.1002/anie.202006727
45. Liu Y., Duan Z., Fang J., et al. (2020). Cellular synthesis and X-ray crystal structure of a designed protein heterocatenane. *Angew. Chem. Int. Ed.* **59**:16122–16127. DOI:10.1002/anie.202005490
46. Doyle L. A., Takushi B., Kibler R. D., et al. (2023). De novo design of knotted tandem repeat proteins. *Nat. Commun.* **14**:6746. DOI:10.1038/s41467-023-42388-y
47. Zhang F., Liu Y., Da X.-D., et al. (2024). Toward selective synthesis of protein olympiadanes via orthogonal active templates in one step. *CCS Chem.* **6**:1047–1059. DOI:10.31635/ccschem.023.202303071
48. Qu Z., Xu L., Jiang F., et al. (2024). Folds from fold: Exploring topological isoforms of a single-domain protein. *Proc. Natl. Acad. Sci. USA* **121**:e2407355121. DOI:10.1073/pnas.2407355121
49. Xu L., Song X., Xu H., et al. (2026). Computational design and cellular synthesis of two protein topological isomers: Solomon link vs. *three-twist knot. Proc. Natl. Acad. Sci. USA* **123**:e2537891123. DOI:10.1073/pnas.2537891123
50. Wang X.-W. and Zhang W.-B. (2017). Protein catenation enhances both the stability and activity of folded structural domains. *Angew. Chem. Int. Ed.* **56**:13985–13989. DOI:10.1002/anie.201705194
51. Wu W.-H., Bai X., Shao Y., et al. (2021). Higher order protein catenation leads to an artificial antibody with enhanced affinity and *in vivo* stability. *J. Am. Chem. Soc.* **143**:18029–18040. DOI:10.1021/jacs.1c06169
52. Liu Y., Bai X., Lyu C., et al. (2022). Mechano-bioconjugation strategy empowering fusion protein therapeutics with aggregation resistance, prolonged circulation, and enhanced antitumor efficacy. *J. Am. Chem. Soc.* **144**:18387–18396. DOI:10.1021/jacs.2c06532
53. Liu Y., Tian X., Zhang F., et al. (2024). Probing the topological effects on stability enhancement and therapeutic performance of protein bioconjugates: Tadpole, macrocycle versus figure-of-eight. *Adv. Healthc. Mater.* **13**:e2400466. DOI:10.1002/adhm.202400466
54. Qu Z., Fang J., Wang Y.-X., et al. (2023). A single-domain green fluorescent protein catenane. *Nat. Commun.* **14**:3480. DOI:10.1038/s41467-023-39233-7
55. Fang J., Li T., Lee J., et al. (2023). A single-domain protein catenane of dihydrofolate reductase. *Natl. Sci. Rev.* **10**:nwad304. DOI:10.1093/nsr/nwad304
56. Shah N. H., Eryilmaz E., Cowburn D., et al. (2013). Naturally split inteins assemble through a "capture and collapse" mechanism. *J. Am. Chem. Soc.* **135**:18673–18681. DOI:10.1021/ja4104364
57. Moro A., Gao Z., Wang L., et al. (2022). Dynamic transcriptional activity and chromatin remodeling of regulatory T cells after varied duration of interleukin-2 receptor signaling. *Nat. Immunol.* **23**:802–813. DOI:10.1038/s41590-022-01179-1
58. Raeber M. E., Rosalia R. A., Schmid D., et al. (2020). Interleukin-2 signals converge in a lymphoid-dendritic cell pathway that promotes anticancer immunity. *Sci. Transl. Med.* **12**:eaba5464. DOI:10.1126/scitranslmed.aba5464
59. Zhang X., Miao M., Zhang R., et al. (2022). Efficacy and safety of low-dose interleukin-2 in combination with methotrexate in patients with active rheumatoid arthritis: A randomized, double-blind, placebo-controlled phase 2 trial. *Signal Transduct. Target. Ther.* **7**:67. DOI:10.1038/s41392-022-00887-2
60. He J., Chen J., Miao M., et al. (2022). Efficacy and safety of low-dose interleukin 2 for primary Sjögren Syndrome: A randomized clinical trial. *JAMA Netw. Open* **5**:e2241451. DOI:10.1001/jamanetworkopen.2022.41451
61. Zhou H., Zhao X., Zhang R., et al. (2023). Low-dose IL-2 mitigates glucocorticoid-induced Treg impairment and promotes improvement of SLE. *Signal Transduct. Target. Ther.* **8**:141. DOI:10.1038/s41392-023-01350-6
62. Xie Y., Wei C., Fu D., et al. (2025). Large-scale multicenter study reveals anticitrullinated SR-A peptide antibody as a biomarker and exacerbator for rheumatoid arthritis. *Sci. Adv.* **11**:eadr8078. DOI:10.1126/sciadv.adr8078
63. Odegard J. M., Marks B. R., DiPlacido L. D., et al. (2008). ICOS-dependent extrafollicular helper T cells elicit IgG production via IL-21 in systemic autoimmunity. *J. Exp. Med.* **205**:2873–2886. DOI:10.1084/jem.20080840
64. Wang D., Fu B., Shen X., et al. (2021). Restoration of HBV-specific CD8(+) T-cell responses by sequential low-dose IL-2 treatment in non-responder patients after IFN-alpha therapy. *Signal Transduct. Target. Ther.* **6**:376. DOI:10.1038/s41392-021-00776-0
65. Zhou P., Chen J., He J., et al. (2021). Low-dose IL-2 therapy invigorates CD8+ T cells for viral control in systemic lupus erythematosus. *PLoS Pathog.* **17**:e1009858. DOI:10.1371/journal.ppat.1009858
66. Rajendiran A. and Tenbrock K. (2021). Regulatory T cell function in autoimmune disease. *J. Transl. Autoimmun.* **4**:100130. DOI:10.1016/j.jtauto.2021.100130

FUNDING AND ACKNOWLEDGMENTS

This work was supported by the financial support from the National Natural Science Foundation of China (No. 21991132, 21925102, 92056118, 22101010, 82071813, 82672341 and 22401013), Shenzhen Medical Research Fund (No. B2302037), International Science and Technology Cooperation Program (Hong Kong, Macao and Taiwan) (Z251100007125012), Beijing Sci-Tech Program (Z191100006619114), Clinical Medicine Plus X project of Peking University, and Beijing National Laboratory for Molecular Sciences (BNLMS-CXXM-202006). W.-B.Z. acknowledges Bayer Pharma for the Bayer Investigator Award. J. F. acknowledges Peking University for Boya Postdoctoral Fellowship. The funders had no role in study design, data collection and analysis, decision to publish, or preparation of the manuscript.

AUTHOR CONTRIBUTIONS

W.-B.Z., J.H. and Z.L. conceived the project and directed the research. J.F. designed the catenane and carried out cellular synthesis and molecular characterizations of topological IL-2 variants. X.T. performed the pharmacokinetic experiments and affinities characterizations. R.F., X.X. and X.T. performed the *in vivo* and *in vitro* experiments in different models and analyzed the data. Y.D. and J.L. performed RNA-sequencing and analyzed the data. J.F., X.T., X.X., R.F., Z.L., J.H and W.-B.Z. prepared the manuscript with contributions from all authors. All authors contributed to the manuscript and approved the final version.

DECLARATION OF INTERESTS

W.-B. Z., Z.L., J.H., J.F., X.X., X.T., and R.F. are authors on a patent regarding these topological IL-2 variants as therapeutic agents for autoimmune diseases (Chinese Patent No.: CN 202310827760.9).

ETHICAL STATEMENT AND PATIENT CONSENT

The study protocols were approved by the Institutional Ethics Committee of Peking University (2021PHE026) and the ethics committee of Peking University People's Hospital (2023PHB093-001).

DATA AND CODE AVAILABILITY

Data are available from the corresponding author upon reasonable request.

SUPPLEMENTAL INFORMATION

It can be found online at https://doi.org/10.59717/j.xinn-life.2026.100259.